INTERNATIONAL JOURNAL OF AUTOMOTIVE AND MECHANICAL ENGINEERING (IJAME)
ISSN: 2229-8649 e-ISSN: 2180-1606
VOL. 19, ISSUE 2, 9773 – 9789
DOI: https://doi.org/10.15282/ijame.19.2.2022.12.0754

ORIGINAL ARTICLE

Heat Transfer and Exergy Analysis of a Shell and Tube Heat Exchanger using PGW based ZnO Nanofluids

U.D. Das, M.A. Mowazzem Hossain*, J.U. Ahamed and M.E.A. Razzaq

Department of Mechanical Engineering, Chittagong University of Engineering & Technology, Chattogram-4349, Bangladesh
Phone: +8801735530848

ABSTRACT – In this experimental work, ZnO nanoparticles were synthesized using the chemical precipitation method, and the nanoparticle structure and morphology were characterized through XRD and SEM. Heat transfer and exergetic characteristics were then studied in a shell and tube heat exchanger using PGW-based ZnO nanofluids varying nanoparticle volume concentration and nanofluid (shell side) flow rate at 6, 8, 10 and 12 litres/min. The hot water flow rate was fixed at 12 litres/min. The experimental results show that the heat transfer rate was improved by increasing the nanoparticle concentration and nanofluid flow rate. When the nanoparticle volume concentration was 0.3 per cent, the maximum enhancement of heat transfer rate and average heat transfer coefficient using ZnO nanofluids were 35.9 per cent and 40.2 per cent, respectively, in comparison to the base fluid. Exergy loss and dimensionless exergy loss both increased with nanofluid flow rate and dropped substantially with increased nanoparticle volume concentrations. The average increment of exergetic effectiveness at three different nanoparticle volume concentration (0.1%, 0.2%, and 0.3%) are 10.68%, 23.64%, and 31.23% respectively. The highest exergetic sustainability index (0.41) and lowest environmental impact factor (2.42) were observed when the nanoparticle concentration was 0.3% with the nanofluid flow rate of 6 litres/min.

ARTICLE HISTORY
Received: 16th Oct. 2021
Revised: 15th June 2022
Accepted: 25th June 2022
Published: 30th June 2022

KEYWORDS
Heat transfer;
Propylene glycol;
Zinc oxide;
Nanofluids;
Exergy

INTRODUCTION

With an increasing emphasis on global warming, greenhouse gas effects, as well as energy concerns, a more efficient heat exchanger system is required to transfer heat effectively. The properties of heat transfer fluids like thermal and physical properties are vital factors that determine the performance of the heat exchanger. There are several methods for enhancing the performance of the heat exchanger, such as the application of fins, usage of microchannels and increasing the heat transfer area. Heat transferability can also be increased by improving the thermal conductivity of the working fluid [1-3]. In recent years, high thermal conductivity solid particles blended into heat transfer fluids have been considered to enhance the heat transfer performance of the fluids. However, suspended micrometre or millimetre-sized particles may cause a variety of problems, including high-pressure drop, clogging, abrasion, and particle sedimentation. The addition of nanoparticles (mean size less than 100 nm) into the fluid instead of large suspended particles may overcome these obstacles [4]. Nanofluids [5] are colloidal suspensions of different types of nanoparticles in the base fluid, which can be used in various engineering applications and are expected to replace conventional fluids soon [6].

A conventional nanofluid is produced by dispersing particular types of selected nanoparticles into an appropriate base fluid with different volume concentrations. The commercial coolants made of water and antifreeze (ethylene glycol and propylene glycol) are used fluid in a variety of industrial applications, including automobiles as engine coolants, coolants for electronic equipment, and industrial heating. Note that ethylene glycol-water mixture (EGW) has better physical properties than propylene glycol-water mixture (PGW). In contrast, EGW is very toxic. Hence, PGW is used in situations where toxicity might be a concern [7]. It is important to note that the PGW solution is generally known to be safe for use in food processing applications. There has been a lot of research using water, Ethylene Glycol, or EGW mixture as working fluid. Nevertheless, in the open literature, similar studies on PGW-based nanofluids are scarce. Devireddy et al. [6] studied the heat transfer rate of EGW (40% ethylene glycol and 60% water) mixture-based TiO_2 nanofluids as an automobile coolant and found that the maximum heat transfer rate was enhanced by about 37% compared to the base fluid. Jiang et al. [8] used distilled water-based Al_2O_3 nanofluids and PGW-based ZnO nanofluids to numerically examine the heat transfer and flow rate in a rectangular cavity. Their findings indicated that the convective intensity and heat transfer performance of distilled water-based Al_2O_3 nanofluids show a nonmonotonic transition as the volume fraction of nanoparticles increases, while the convective intensity and heat transfer performance of nanofluid PGW–ZnO decreases monotonously.

Although numerous experimental studies have been conducted to estimate the heat transfer characteristics of nanofluids in several sorts of heat exchangers [9–14], relatively little work has been related to shell and tube heat exchangers in the open literature. Elias et al. [15] analyzed the effect of various nanoparticle shapes on the performance of shell and tube heat exchanger by using water and ethylene glycol mixture based on γ-AlOOH nanofluid analytically.

*CORRESPONDING AUTHOR | M.A. Mowazzem Hossain | ✉ mowazzem@cuet.ac.bd

Their results found that a cylindrical shape had greater heat transfer characteristics and a faster heat transfer rate among the five nanoparticle shapes. The thermal performance of different types of nanoparticles (Fe_3O_4, ZnO, TiO_2, CuO, and Al_2O) in the shell and tube heat exchanger was investigated by Shahrul et al. [3]. In their experiment, the author showed that the highest energy effectiveness was found in the ZnO nanofluid, whereas the Al_2O_3 nanofluid shows the highest heat transfer coefficient. Farajollahi et al. [16] compared the heat transfer characteristics of water-based γ-Al_2O_3 and TiO_2 nanofluids in the shell and tube heat exchanger. Their results suggest that TiO_2 nanofluids have greater heat transfer properties compared to Al_2O_3 nanofluids. Fares et al. [17] investigated the convective heat transfer coefficient in a vertical type shell and tube heat exchanger using graphene nanofluids. Their findings revealed that using 0.2 percent graphene/water nanofluids can increase the heat transfer coefficient by up to 29 percent while increasing the mean thermal efficiency by 13.7 percent. The effects of water-based MWNT (multi-walled carbon nanotube) nanofluid on heat transfer enhancement in a horizontal type shell and tube heat exchanger were examined by Lotfi et al. [18]. The results revealed that heat transfer increases with multi-wall nanotubes in comparison with the base fluid. Albadr et al. [19] investigated convective heat transfer and flow characteristics of a water-based Al_2O_3 nanofluid in the horizontal type shell and tube heat exchanger. The heat transfer coefficient improved slightly according to the results of their experimental study. Ghozatloo et al. [20] analyzed the convective heat transfer coefficients in a shell and tube heat exchanger using graphene/water nanofluids under laminar flow. The results showed a significant amount of augmentation in the convective heat transfer coefficient of up to 35.6% as compared to the base fluid.

Nowadays, the energy crisis has become a major concern for a developing country like Bangladesh. To emerge from the energy crisis, we need adequate information on energy uses and losses. Energy analysis only shows how much energy is consumed and how much energy is lost from a system. But that doesn't give us a lot of information on the internal inefficiency of the equipment. Moreover, because of the irreversible nature of the system and the system environment, energy analysis is inadequate. On the other hand, exergy analysis can give us information about the usable work potential or exergy of a system [21,22]. It has also been studied that the system with the highest and lowest exergy destroyed in a system can be used to improve the performance of the system. In this respect, exergy analysis is currently a popular topic of research all over the world, and it has a good prospect in the field of sustainable green energy. Although several studies have been conducted on energy and exergy analysis of a system [23,24], work related to exergy analysis in shell and tube heat exchanger was relatively less in the open literature. Durmuş [25] investigated heat transfer, exergy, and pressure loss in a heat exchanger (with and without cut-out conical turbulators). Dizaji et al. [26] studied the effects of water (hot or cold) flow rates, temperature, and geometrical parameters on exergy loss, dimensionless exergy loss, and exergetic effectiveness for a TTHC heat exchanger. In their study, the authors showed that the amount of exergy loss rises with the increment of hot or cold-water flow rates, the inlet temperature of hot water, and coil diameter. Khairul et al. [27] investigated the effects of water-based CuO nanofluids on exergy loss in the corrugated plate heat exchanger. Their experimental results showed that the exergy destruction was significantly reduced using nanofluids compared to the base fluid. Esfahani et al. [28] used graphene oxide nanofluid to investigate the exergy loss in a shell and tube heat exchanger. The author claimed that the exergy loss was greatly reduced under both laminar and turbulent conditions by using graphene oxide nanofluids as the hot fluid.

This experimental study attempts to analyze the heat transfer rate, overall heat transfer coefficient, energy effectiveness, exergy loss, dimensionless exergy loss, exergetic effectiveness, exergetic sustainability index (SI), and environmental impact factor (EIP) at different nanofluid (cold fluid) flow rates and nanoparticle volume concentrations in a shell and tube heat exchanger using propylene glycol and water mixer (PGW)-based ZnO nanofluid. In this study, the nanofluid was prepared using 40% propylene glycol and 60% water with three different volume concentrations (0.1%, 0.2%, and 0.3%) of ZnO nanoparticles by using the two-step method. The flow rate of the nanofluid (shell side) was set at 6, 8, 10, and 12 liters/min. The flow rate of hot fluid was kept constant at 12 liters/min.

MATERIALS AND METHODS

Materials

Extra-pure ZnO powders were obtained from Taj Scientific, Chittagong, Bangladesh (manufactured by PT. Smart-Lab, Indonesia). Analytical grade NH_4HCO_3 was purchased from Jonaki Scientific Store, Dhaka, Bangladesh (manufactured by Loba Chemie Pvt. Ltd., India).

ZnO Nanoparticle Synthesis and Characterization

In this paper, the zinc oxide nanoparticles have been synthesized using a simple method named chemical precipitation technique [29] that is cost-effective, able to synthesize at a large volume, and environmentally friendly. According to our lab facility, the method of the synthesis process was slightly modified. At first, 120 ml of distilled water was put into a 500 ml beaker, and 96 gm of ammonium bicarbonate was dissolved in distilled water. Then 16 gm of ZnO powder was added to the prepared NH_4HCO_3 solution and stirred with a glass rod for approximately 5-6 min to dissolve ZnO completely in the solution. The beaker was then placed on the hot plate stirrer (magnetic stirrer with hot plate), and 32 gm of ZnO powder was added to the solution under stirring at 60 °C. After two hours, the beaker was put down from the hot plate stirrer and white precipitates were dried in a water bath at about 70 °C for 10 hours. The resulting product was then calcined at 400 °C for about 1 hour 30 mins. The whole process of synthesizing ZnO nanoparticles is presented in a schematic diagram (Figure 1). After calcination, the final product was well ground using mortar and pestle. The reactions occurring in the ZnO formation are shown in the Eq. (1) to Eq. (4) [29].

$$NH_4HCO_3 + H_2O \longrightarrow NH_4^+ + HCO_3^- + NH_3 + CO_3^{2-} + OH^- \quad (1)$$

$$NH_4^+ + HCO_3^- + NH_3 + CO_3^{2-} + OH^- \longrightarrow \underbrace{NH_3;\ NH_4OH;\ (NH_4)_2CO_3;\ NH_4HCO_3;\ H_2O}_{\textbf{AHCH}\ \text{(Ammonium hydrogen carbonate solution)}} \quad (2)$$

$$ZnO + AHCH \longrightarrow ZnO\downarrow + xNH_3\uparrow + yH_2O\uparrow + zCO_2\uparrow + Zn_5(OH)_6(CO_3)_2\downarrow \quad (3)$$

The results of XRD show that precipitated $Zn_5(OH)_6(CO_3)_2$ completely converts into zinc oxide after calcination at 400 °C.

$$Zn_5(OH)_6(CO_3)_2 \longrightarrow 5ZnO + 2CO_2 + 3H_2O \quad (4)$$

In this experimental study, the crystal structure and microstructure of the synthesized and ZnO nanoparticles were investigated using XRD (GBC scientific; Cu_$K_{\alpha 1}$: λ = 1.54062A° radiation source) and SEM (model: JSM 7600F, JEOL-Japan). The crystallite size ZnO nanoparticles were evaluated using the Debye-Scherrer formula, Williamson-Hall method, and the Size-strain plot method (SSP).

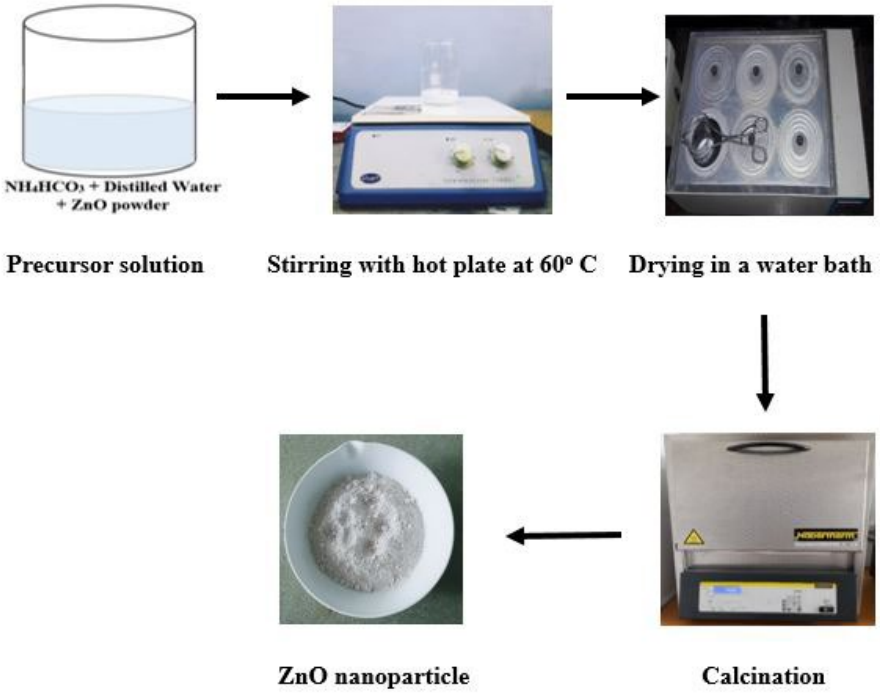

Figure 1. Schematic representation of ZnO nanoparticle synthesis process.

Preparation of ZnO Nanofluid

In this study, the nanofluid was prepared using 40% propylene glycol and 60% water with different volume concentrations of ZnO nanoparticles by using the two-step method. The required amount of nanoparticles for the preparation of the nanofluid of a particular volume fraction, using PGW (40:60) mixture as base fluid was calculated by using the following relation:

$$\%\ \text{vol. concentration}, \varphi = \frac{\frac{w_{nanoparticle}}{\rho_{nanoparticle}}}{\frac{w_{nanoparticle}}{\rho_{nanoparticle}} + \frac{w_{base\ fluid}}{\rho_{base\ fluid}}} \quad (5)$$

The required nanoparticles were added with the 1 liter base fluid, and the solution was subjected to the mixing process using a magnetic stirrer for 10 hours and then underwent a sonication process using an ultrasonic bath for 1 hour. No surfactant was used as it could deteriorate the thermal properties of the nanofluid [30]. A total of 5 liters nanofluid of a

particular volume concentration was prepared for the present investigation. In this study, three different volume concentration (0.1%, 0.2%, and 0.3%) of ZnO nanoparticles were used. The components and process of nanofluid preparation are shown in Figure 2.

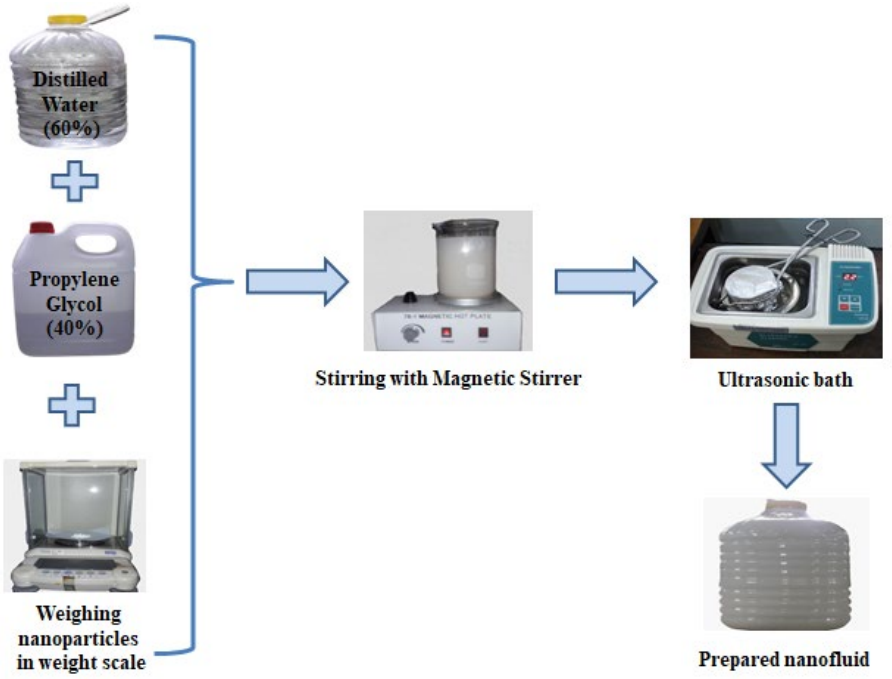

Figure 2. ZnO nanofluids preparation process.

Experimental Setup and Procedure

For experimental, an NFU-type shell and tube heat exchanger was used. The heat exchanger had two tubes inside a cylindrical shell. The heat exchanger was made of stainless steel. Each tube was 0.49 m long and had inside and outside diameters of 0.009 m and 0.0095 m, respectively. The cylindrical shell had a 0.15 m outer diameter and it was 0.3045 m long. According to the flow arrangement, it was a parallel flow type heat exchanger. A shell and tube heat exchanger was modeled in SolidWorks, as shown in Figure 3.

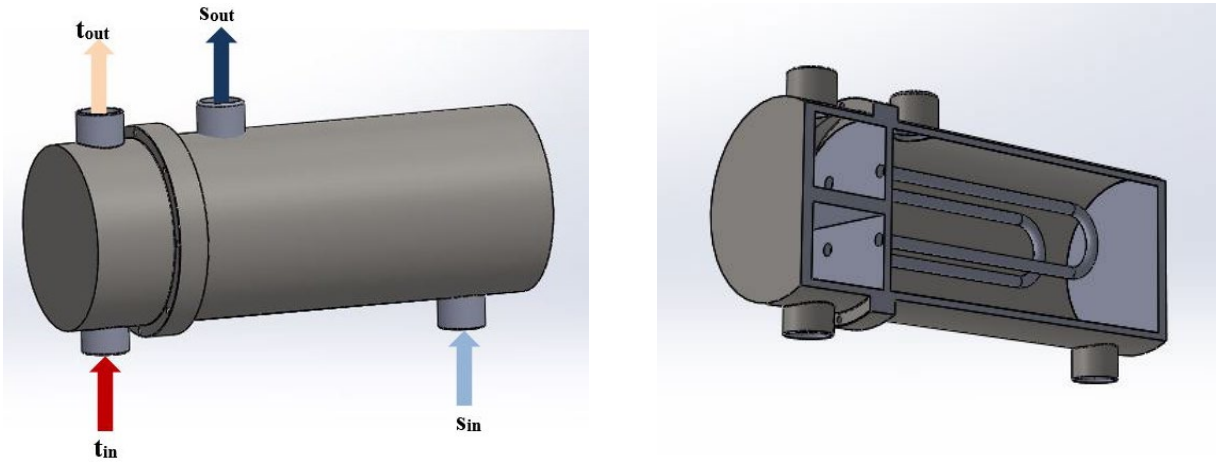

(a) (b)

Figure 3. Solidworks model of the test section (a) Shell and tube heat exchanger and (b) Section view of a heat exchanger.

In this experimental investigation, an experimental setup of shell and tube heat exchanger was developed to analyze the effects of (PGW) -based ZnO nanofluid on the heat transfer performance. It consisted of a hot fluid tank, a cold fluid tank, two 0.5 hp centrifugal pumps (RFL Water Pump, Centrifugal 1 "X1"-0.5HP (RCm-130)), two flow measuring devices (PRM FMZ400410GPM 1-10 GPM Water Rotameter Flow Meter, ± 4% accuracy), two flow control valves, an electric heater, pipes, joints, etc. The experimental setup was well insulated by using insulation tape, glass wool, and aluminum foil to eliminate the heat loss between the test rig and the surrounding. The specifications of the water pumps used in this experiment are shown in Table 1. A schematic diagram and an actual image of the experimental setup are shown in Figures 4 and 5, respectively.

Table 1. Specifications of water pumps used in this experimental study.

Specifications	Value
Model	BBY03343
Motor power	0.5 hp (0.37 KW)
Motor voltage	220 V
Max. head	24 m
Max. flow rate	50 L/min
Sn.	1 inch
Dn.	1 inch

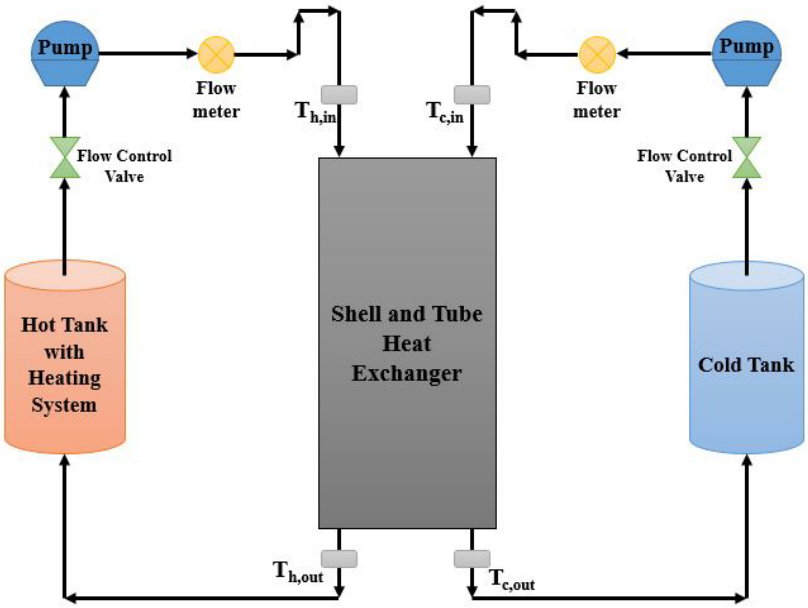

Figure 4. Schematic of the experimental layout.

In Figure 5, two buckets were connected in a closed-loop with the heat exchanger where in one there was nanofluid (coolant) and in another, there was hot water that was heated by using an electric heater. Both the hot water and nanofluid were circulated by two different pumps through a pipe of 1-inch diameter. Hot water was circulated in the tube side and nanofluid was circulated in the shell side. The volume flow rate was measured using two flow meters (rotameter) which were connected to the loop. Gate valves were used for changing the flow rate. The flow rate of hot fluid was kept constant at 12 Liters/min. In this experiment, the flow rate of nanofluid was varied at 6, 8, 10, and 12 liters/min. There were four N2 filled Laboratory Thermometer (ZEAL, made in England, range: -10 to 110 ºC (0.1 ºC)) inserted in the pipe at both inlet and outlet of the nanofluid and hot water to measure the required temperatures. The data were collected when the flows were in steady condition.

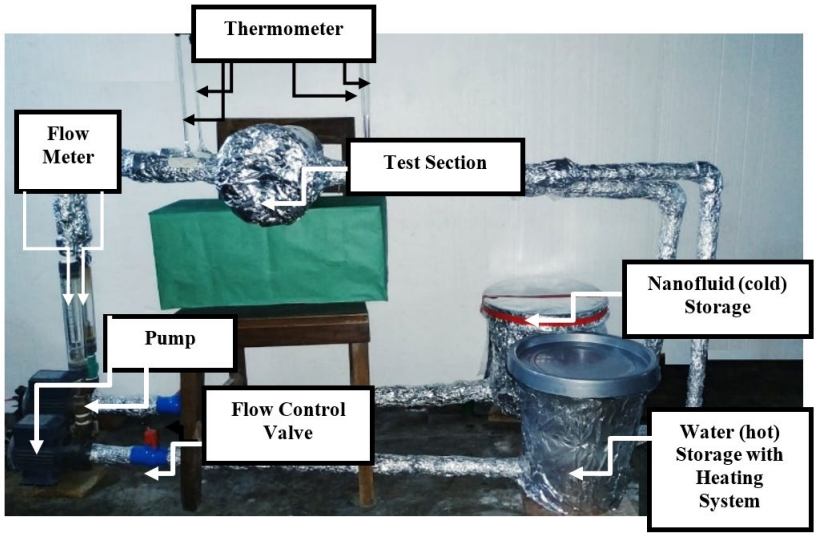

Figure 5. Image of experimental setup.

CALCULATION METHOD

Structural Studies

Lattice parameter unit volume

The lattice parameters ($a = b$ and c) were estimated using Miller indices <*hkl*> and *d* spacing according to the following relations since the crystal structure of the ZnO nanoparticle is a hexagonal wurtzite structure [31]. For the <100> plane, the lattice parameter 'a' can be calculated by

$$a = \frac{\lambda}{\sqrt{3}\sin\theta} \tag{6}$$

And the lattice parameter 'c' for the <002> plane, is estimated by

$$c = \frac{\lambda}{\sin\theta} \tag{7}$$

The unit cell volume of the fabricated ZnO nanoparticles can be calculated using the following relation [31]:

$$V = \frac{\sqrt{3}a^2c}{2} \tag{8}$$

Now, the Zn–O bond length L can be calculated by

$$L = \sqrt{\left(\frac{a^2}{3} + \left(\frac{1}{2} - u\right)^2\right)c^2} \tag{9}$$

where u is the wurtzite structure's positional parameter [31] and may be calculated by

$$u = \frac{a^2}{3c^2} + 0.25 \tag{10}$$

Crystallite Size Analysis

Scherrer method

The average crystallite size of the as-prepared ZnO particles was estimated by using the Debye-Scherrer formula [32] as

$$D = \frac{k\,\lambda}{\beta\,cos\theta} \tag{11}$$

where D is the crystallite size, λ is the X-ray wavelength (0.154062nm), k is the Scherrer constant (0.89), β is FWHM (full width at half maximum). The inter-planar spacing between atoms (d-spacing) can be calculated by Bragg's Law (Eq. (12)).

$$2d\sin\theta = n\lambda \tag{12}$$

here, θ is diffraction angle, and d is interplanar spacing.

Williamson-Hall method

A perfect crystal is one in which all atoms are in their ideal position and has no imperfections. According to Williamson-Hall, crystal is imperfect due to the size of the finite crystal and their corresponding lattice strain(ε) [33]. Williamson–Hall plot equation to estimate the crystallite size and lattice strain of the samples is as follow [34]:

$$\beta\cos\theta = \frac{k\,\lambda}{D} + 4\varepsilon\sin\theta \tag{13}$$

The above equation is also referred to as Uniform Deformation Model (UDM). Here, the crystal is regarded as isotropic and it is presumed that the material properties are not dependent on the crystallographic directions [31].

Size-strain plot method (SSP)

The size–strain parameters can also be found by using the 'Size–Strain Plot' (SSP) method. It provides a more accurate evaluation of size-strain parameters where the strain profile is expressed by the Gaussian function and the crystallite size by the Lorentzian function[31,35].

$$(d_{hlk}\beta_{hkl}\cos\theta_{hkl})^2 = \frac{1}{v_s}\left(d_{hkl}^2\beta_{hkl}\cos\theta_{hkl}\right) + \left(\frac{\varepsilon_a}{2}\right)^2 \tag{14}$$

where d_{hkl} is the interplanar lattice spacing, v_s is the apparent volume-weighted average size, and ε_a is the apparent strain. For spherical crystallites, the crystallite size can be determined by [31].

$$D_v = \frac{3}{4}v_s \tag{15}$$

Hence, we can determine crystallite size from the slope of the linear fit and from the y-intercept, find out the strain value.

Physical Properties

The Pak and Cho [36] Eq. (16), was employed to evaluate the density of nanofluid in this experimental study. The specific heat of nanofluids was estimated using the Eq. (17) which was developed by Zhou et al. [37] and is favorable for a wide range of volume concentrations [38,39]. The Maxwell equation in Eq. (19) was used to determine the thermal conductivity of nanofluids, and the dynamic viscosity of nanofluids was used to estimate using Eq. (18) which was developed by Naik and Syam Sundar [38,40]. The measured thermo-physical properties [3,41-43] of nanoparticle, water, and PGW mixture (base fluid) are presented in Table 2.

$$\rho_{nf} = \varphi\rho_{np} + (1-\varphi)\rho_{bf} \tag{16}$$

$$C_{p,nf} = \frac{\varphi(\rho Cp)_{np} + (1-\varphi)(\rho Cp)_{bf}}{\rho_{nf}} \tag{17}$$

$$\mu_{nf} = \mu_{bf}(1 + 2.5\varphi + 6.2\varphi^2) \tag{18}$$

$$K_{nf} = K_{bf}\frac{K_{np} + 2K_{bf} - 2\varphi(K_{bf} - K_{np})}{K_{np} + 2K_{bf} + \varphi(K_{bf} - K_{np})} \tag{19}$$

Table 2. Thermo-physical properties of nanoparticle, water, and base fluid.

Material	Density (kg/m^3)	Specific heat (J/Kg K)	Thermal conductivity (W/m K)	Dynamic viscosity (Pa.s)
ZnO	7133	383	111	0.5606
Water	998.9	4181	0.613	0.00894
PGW (40:60)	1026.5	3747.186	0.388	0.58

Thermal Performance

The heat transfer rate of the cold fluid (nanofluid) can be expressed as

$$\dot{Q}_c = \dot{m}_c C_{pc}(T_{c,out} - T_{c,in}) \tag{20}$$

where $\dot{m}_c$ is the mass flow rate of nanofluid, C_{pc} is the specific heat of nanofluid, $T_{c,in}$ and $T_{c,out}$ are the inlet and outlet temperature of the nanofluid respectively.

Overall heat transfer coefficient of nanofluid can be expressed as

$$U_0 = \frac{\dot{Q}_c}{A_o F \Delta T_m} \tag{21}$$

where ΔT_m is the log mean temperature difference, A_0 is the total tube area (outer side), and F is the LMTD correction factor can be obtained from Holman et al. [44] chart. Effectiveness of an NFU type shell and tube heat exchanger can be expressed as:

$$\varepsilon = \frac{\text{Actual heat transfer rate}}{\text{Maximum possible heat transfer rate}} = \frac{\dot{Q}}{\dot{Q}_{max}} \tag{22}$$

where,

$$\dot{Q} = \dot{m}_c C_{pc} \, (T_{c,out} - T_{c,in}) = \dot{m}_h C_{ph} \, (T_{h,out} - T_{h,in}) \tag{23}$$

$$\dot{Q}_{max} = C_{min} \, (T_{h,in} - T_{c,in}) \tag{24}$$

here, C_{min} = The smaller of $\dot{m}_c C_{pc}$ and $\dot{m}_h C_{ph}$

Exergy Analysis

The following equation can be used to evaluate the amount of exergy loss in a steady-state open system[26]:

$$E = T_e \left[\dot{m}_h C_{ph} \ln \left(\frac{T_{h,out}}{T_{h,in}} \right) + \dot{m}_c C_{pc} \ln \left(\frac{T_{c,out}}{T_{c,in}} \right) \right] \tag{25}$$

The dimensionless exergy loss can be determined as [24]

$$e = \frac{E}{\dot{m}_h \, C_{ph} \left\{ \Delta T_h - T_e \left[ln \left(\frac{T_{h,out}}{T_{h,in}} \right) \right] \right\}} = \frac{E}{\dot{m}_h \, C_{ph} \left\{ (T_{h,in} - T_{h,out}) - T_e \left[ln \left(\frac{T_{h,out}}{T_{h,in}} \right) \right] \right\}} \tag{26}$$

The exergetic effectiveness (second law efficiency) for a system that does not participate in the generation or input of work (heat exchangers) can be defined as the achievement of the goal of the process in terms of availability changes or transfers relative to the process input. The second law efficiency of a heat exchanger, where heat energy is exchanged from a high-temperature fluid stream to a low-temperature fluid stream, can be defined as [26]:

$$\eta = \frac{\dot{m}_c \, C_{pc} \left\{ (T_{c,out} - T_{c,in}) - T_e \left[ln \left(\frac{T_{c,out}}{T_{c,in}} \right) \right] \right\}}{\dot{m}_h \, C_{ph} \left\{ (T_{h,in} - T_{h,out}) - T_e \left[ln \left(\frac{T_{h,in}}{T_{h,out}} \right) \right] \right\}} \tag{27}$$

Another parameter that is often used to express exergy performance is the exergetic sustainability index (SI) [45]. The exergetic sustainability index (SI) helps to evaluate the stability of the energy process. The exergetic sustainability index can be calculated by [24]:

$$SI = \frac{\eta}{1 - \eta} \tag{28}$$

The environmental impact factor (EIF), on the other hand, illustrates whether exergy losses affect the environment. Lower EIF indicates that the system is more environmentally friendly. Environmental impact factors can be estimated by [24]:

$$EIF = \frac{1}{SI} \tag{29}$$

RESULTS AND DISCUSSION

XRD Analysis

The XRD data of synthesized ZnO nanoparticles is presented in Table 3 and graphically illustrated in Figure 6. In Figure 6, it has been observed that the characteristic peaks of the hexagonal zinc oxide wurtzite located at 2θ values of 31.8, 34.44, 36.26, 47.54, 56.62, 62.86, 66.4, 67.94, 69.06, and 72.56° which was originated by the reflections from the lattice planes of <100>, <002>, <101>, <102>, <110>, <103>, <200>, <112>, <201> and <004>, respectively. Here, the XRD pattern is consistent with JCPDS data (JCPDS Card No.: 01-089-0510) and also agreed with previously reported data. The sharp and narrow peak intensity confirms that the synthesized ZnO nanoparticle is of high quality with fine grain size and good crystallinity.

Table 4 shows the lattice parameters and unit cell volume of the synthesized ZnO nanoparticles which were determined using Eqs. (6), (7), and (8). The estimated Zn–O bond length is 1.9763 Å, while the reported Zn–O bond length is 1.9767 Å [46]. The measured bond length, lattice parameters, and unit cell volume of the synthesized ZnO nanoparticles are agreed very well with the experimental data of hexagonal wurtzite ZnO [47].

The average crystallite size of the fabricated ZnO nanoparticles was calculated from XRD peak width <101> using the Scherrer formula and tabulated in Table 5. Figure 7 shows the Williamson-Hall (W-H) plot for ZnO nanoparticles. Here, the line through the points has positive slopes and non-zero y-intercepts, implying that they are isotropic in nature.

In Figure 8, a size strain plot was drawn taking $(d_{hkl}\ \beta_{hkl}\ cos\theta_{hkl})^2$ on the y axis and $d^2_{hkl}\beta_{hkl}cos\theta_{hkl}$ on the x-axis for synthesized ZnO nanoparticles. Table 5 shows the crystallite size and strain value which were determined by the Scherrer method, Williamson- Hall, and size-strain plot method. Noted that the crystallite size of the ZnO nanoparticles obtained from the different models is somewhat similar, suggesting that the inclusion of strain in various forms has very little effect on the average crystallite size of ZnO nanoparticles. However, the average crystallite size found from the Scherrer formula shows a large variation with the Williamson- Hall analysis due to the difference in averaging the particle size distribution, while the SSP method shows little variation. It was observed that the result of the SSP model (Figure 8) was more accurate than the UDM (Figure 7), as the data were well closed in the fitting line.

Table 3. XRD data and structural parameters of synthesized ZnO nanoparticles.

Plane (*hkl*)	2θ (degree)	FWHM (radian)	Crystallite size (nm)	Interplanar spacing (Å)
100	31.8	0.00642	22.15	2.81
002	34.44	0.00611	23.74	2.60
101	36.26	0.00735	19.85	2.48
102	47.54	0.00936	16.20	1.91
110	56.62	0.00955	16.48	1.62
103	62.86	0.00881	18.45	1.48
200	66.4	0.00766	21.63	1.41
112	67.94	0.00895	16.56	1.38
201	69.06	0.00895	18.79	1.36
004	72.56	0.01046	16.43	1.30

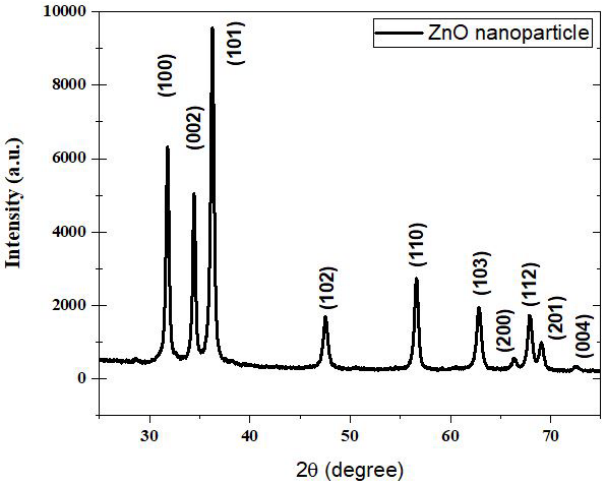

Figure 6. X-ray diffraction pattern of the fabricated ZnO nanoparticle.

Table 4. The lattice parameters and unit cell volume of the synthesized ZnO nanoparticles and their differences with the experimental measurements.

Sample	*a* (nm)	*c* (nm)	V (nm^3)
Synthesized ZnO	0.3247	0.5204	0.04752
Experimental [47]	0.3254	0.5215	0.04782
Deviation (%)	0.154%	0.211%	0.627%

The average crystallite size of the fabricated ZnO nanoparticles was calculated from XRD peak width <101> using the Scherrer formula and tabulated in Table 5. Figure 7 shows the Williamson-Hall (W-H) plot for ZnO nanoparticles. Here, the line through the points has positive slopes and non-zero y-intercepts implying that they are isotropic in nature. In Figure 8, a size strain plot was drawn taking $(d_{hkl}\ \beta_{hkl}\ cos\theta_{hkl})^2$ on the y axis and $d^2_{hkl}\beta_{hkl}cos\theta_{hkl}$ on the x-axis for synthesized ZnO nanoparticles. Table 5 shows the crystallite size and strain value which were determined by the Scherrer method, Williamson-Hall, and size-strain plot method. Noted that the crystallite size of the ZnO nanoparticles obtained from the different models is somewhat similar, suggesting that the inclusion of strain in various forms has very little effect on the average crystallite size of ZnO nanoparticles. However, the average crystallite size found from the Scherrer formula shows a large variation with the Williamson- Hall analysis due to the difference in averaging the particle size distribution, while the SSP method shows little variation. It was observed that the result of the SSP model (Figure 8) was more accurate than the UDM (Figure 7), as the data were well closed in the fitting line.

Table 5. Geometrical parameters of the synthesized ZnO nanoparticles.

Scherrer method	Williamson-Hall plot method (UDM)		Size-strain plot (SSP) method		SEM
D_{avg} (nm)	D (nm)	ε (no unit)	D (nm)	ε (no unit)	D (nm)
19.85	26.02	0.00118	22.71	0.0115	40.96

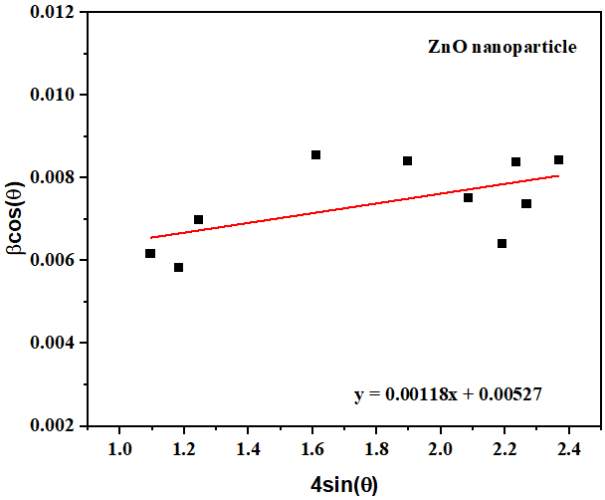

Figure 7. Williamson-Hall plot.

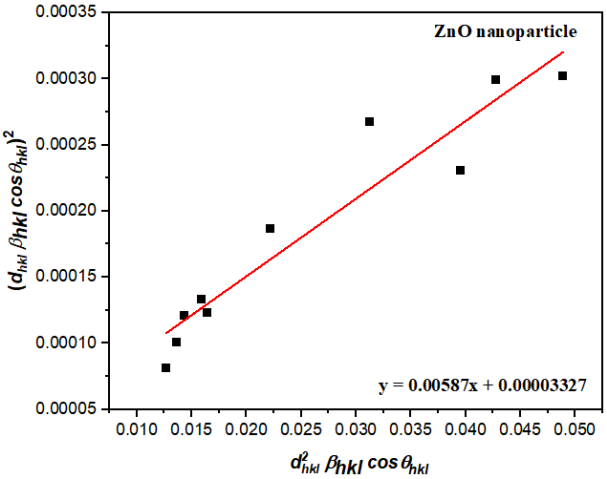

Figure 8. The size-strain plot (SSP).

SEM Analysis

The shape and morphology of ZnO nanoparticles were observed in the FESEM micrograph as shown in Figure 9. The SEM images demonstrate a uniform structure and size for ZnO nanoparticles. It is clearly shown that the particles are predominantly spherical in shape. However, some moderately agglomerated particles and elongated particles are also observed in the SEM images. The average grain size is around 40.96 nm (using ImageJ software). The grain size distribution of the fabricated ZnO nanoparticles is presented in Figure 10.

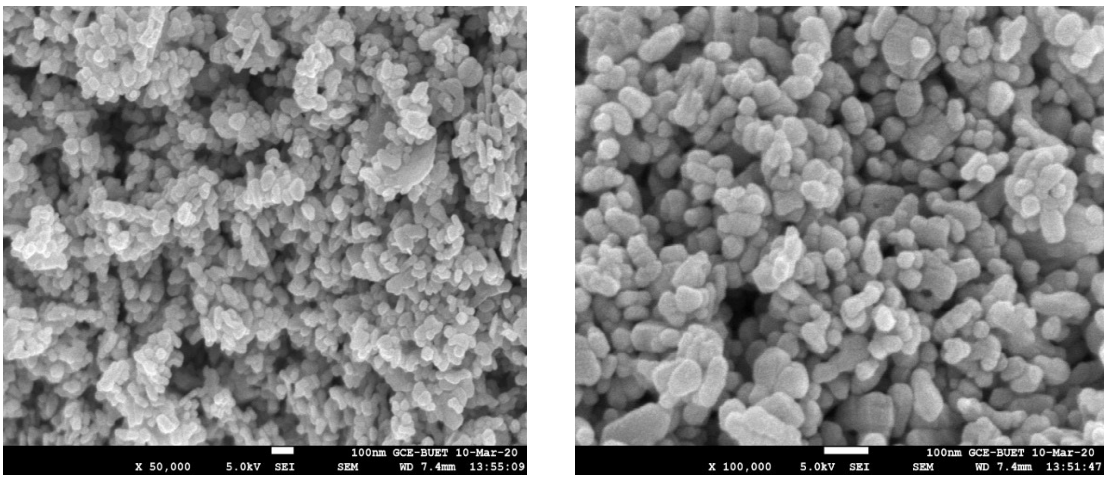

(a) (b)

Figure 9. SEM image of the synthesized ZnO nanoparticles (a) 50,000 magnification and (b) 100,000 magnification.

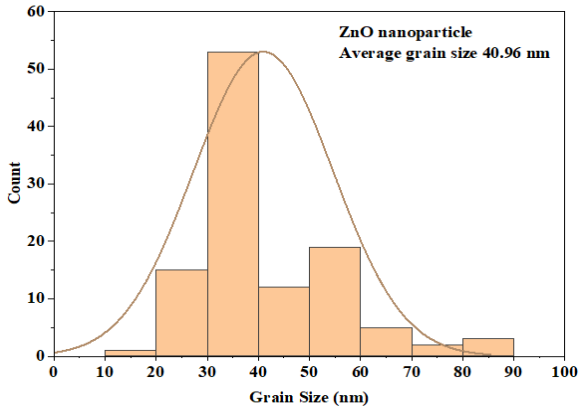

Figure 10. Grain size distribution of the synthesized ZnO nanoparticles.

Stability Analysis of Prepared Nanofluids

The stability check of prepared nanofluids is critical, and several methods, such as sedimentation photograph method, centrifugation method, zeta potential method, electron microscopy method, and so on, have been utilized to examine the stability of nanofluids [40]. In this study, the sedimentation photograph method was employed to observe the nanofluids stability after a 4 hours interval. No surfactant was used in this experiment to prepare the PGW-based ZnO nanofluids (0.1%, 0.2%, and 0.3% volume concentration). However, the stability of PGW-based ZnO nanofluids with and without surfactant (0.1wt% EBT (eriochrome black T)) was examined. This will aid in understanding the influence of EBT surfactant in PGW-based ZnO nanofluids, as well as future research into the effect of EBT surfactant in PGW-based ZnO nanofluids on thermophysical characteristics and heat transfer. Figure 11 depicts the sedimentation of ZnO nanoparticles with and without the use of EBT surfactant. Nanofluids with a volume concentration of 0.1, 0.2, and 0.3% without EBT were all stable till 1 day since no sedimentation occurred. After 2 days, we noticed some sedimentation in the 0.1% concentration, but the 0.2% and 0.3% concentrations remained stable. This is because there were not sufficient nanoparticles to provide adequate repulsive force to form a stable suspension, 0.1% volume concentration nanofluid agglomerate easily compared to 0.2% and 0.3% nanofluids. After 3 days, however, some sediment was observed in the 0.2% and 0.3% concentration nanofluids. The amount of sedimentation was smaller in the case of 0.3% than 0.2%. After 4 days, we noticed more precipitation in 0.3% ZnO nanofluids without surfactant. Regardless of concentration, the nanofluids prepared with 0.1 wt% EBT shows good stability even after 14 days.

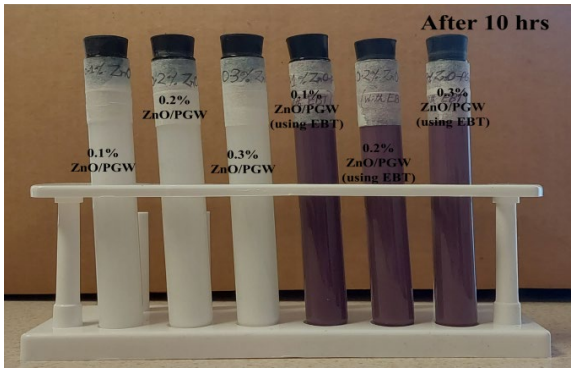

(a)

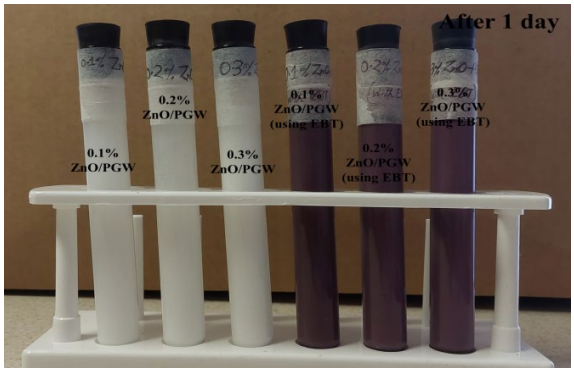

(b)

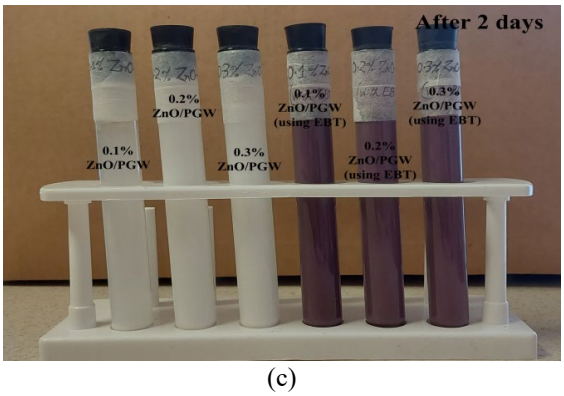

(c)

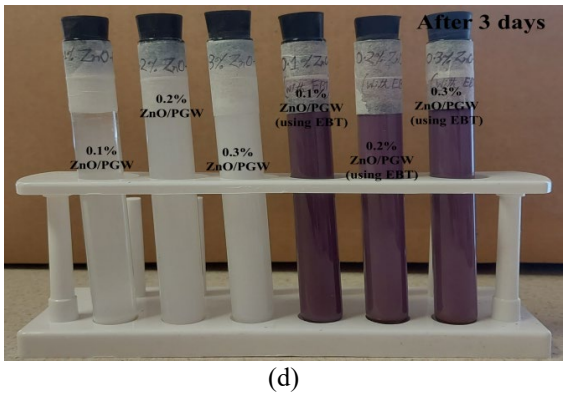

(d)

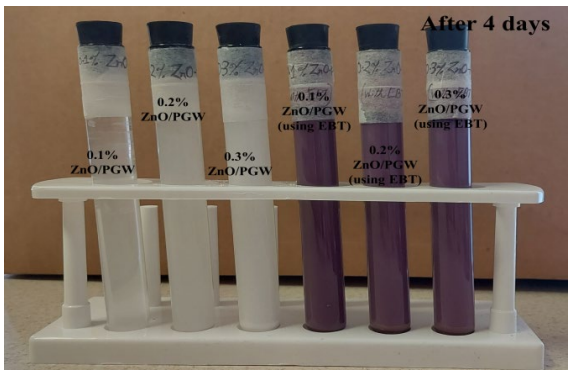

(e)

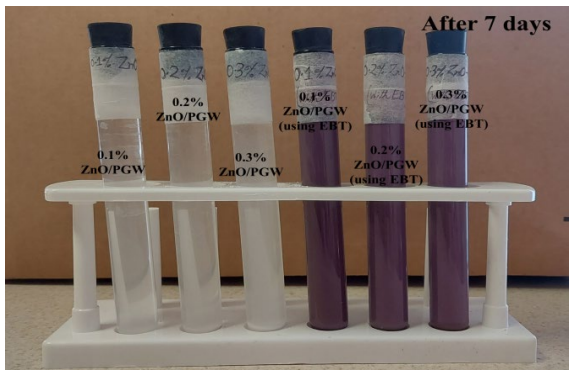

(f)

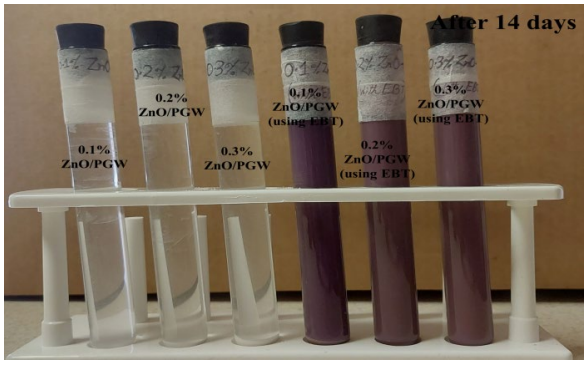

(g)

Figure 11. Sedimentation of ZnO nanoparticles with and without surfactant at different time periods: (a) after 10 hours, (b) after 1 day, (c) after 2 days, (d) after 3 days, (e) after 4 days, (f) after 7 days, and (g) after 14 days.

Heat Transfer Analysis

Figure 12(a) and 12(b) demonstrate the effect of nanoparticle concentration on heat transfer rate and overall heat transfer coefficient. As the nanoparticle volume concentration and nanofluid flow rate increase, so do the heat transfer rate and overall heat transfer coefficient. This could be due to the increased mass flow rate as well as improved thermal conductivity and other thermal properties of the heat transfer fluid as a result of the enhanced collision between nanoparticles, Brownian motion, the effect of nanoparticle clustering, and so on [48]. The maximum value of the heat transfer rate was 464.42 W at 0.3% volume concentration and 12 litres/min flow rate of nanofluid. The average enhancement of heat transfer rate at 0.1%, 0.2%, and 0.3% volume concentration of nanoparticle were 7.51%, 18.23%, and 30.29%, respectively compared to base fluid (PGW). In Figure 13, we can see that the maximum value of the overall heat transfer coefficient was 1077.07 W/m^2.K at 0.3% volume concentration and 12 litres/min flow rate of nanofluid. The average enhancement of overall heat transfer coefficient at 0.1%, 0.2%, and 0.3% nanoparticle volume concentration were 10.64%, 22.2%, and 35.25% respectively. In this experimental study, heat exchanger effectiveness was increased with the increment of nanoparticle volume concentration. A comparison between the enhancement of heat exchanger effectiveness at different nanofluid flow rates and nanoparticle volume concentration was presented in Figure 13. The average enhancement of heat exchanger effectiveness at 0.1%, 0.2%, and 0.3% nanoparticle volume concentration were 10.84%, 21.96%, and 34.96% respectively compared to base fluid. It is interesting to note that the maximum heat exchanger effectiveness was observed at 10 litres/min flow rate of nanofluid.

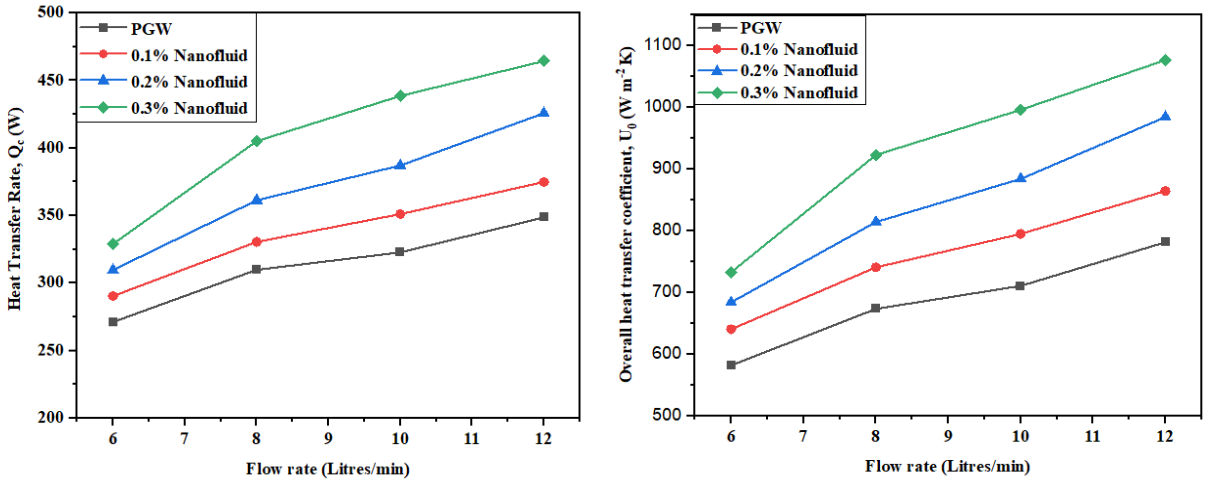

(a) (b)

Figure 12. (a) Heat transfer rate (shell side) and (b) overall heat transfer coefficient (shell side) versus nanofluid flow rate at different nanoparticle volume concentrations.

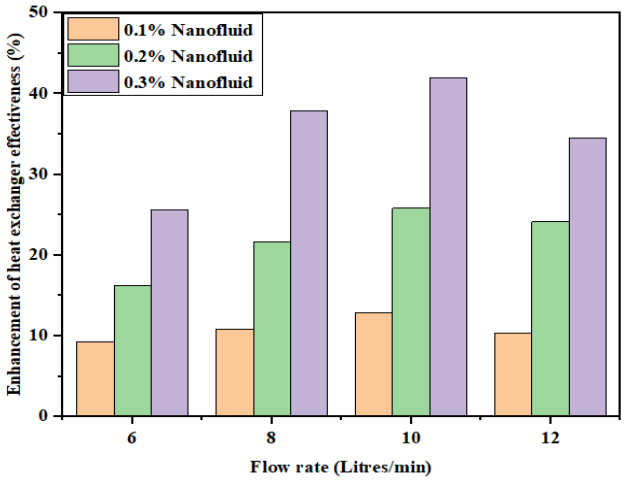

Figure 13. Enhancement of heat exchanger effectiveness with nanofluid flowrate for different nanoparticle volume concentrations.

Exergetic Performance Analysis

The effect of nanoparticle volume concentration and nanofluid flow rate on exergy loss and dimensionless exergy loss are presented in Figures 14(a) and 14(b), respectively. As the flow rate of nanofluid (cold fluid) increases, both exergy loss and dimensionless exergy loss were increased; however, exergy loss and dimensionless exergy loss were significantly reduced with the increment of nanoparticle concentration. This could be due to increased frictional loss as the flow rate increased, increasing the system's irreversibility and, as a result, increasing exergy loss. Adding nanoparticles, on the other hand, improves thermal characteristics, promoting better heat transfer and lowering exergy loss. The average decrement of exergy loss at 0.1%, 0.2%, and 0.3% nanoparticle volume concentration were 11.87%, 28.55%, and 35.9% respectively. The minimum values of dimensionless exergy loss are 0.08 at 0.3% volume concentration and 6 liters/min flow rate of nanofluid when the hot fluid flow rate was constant (12 liters/min).

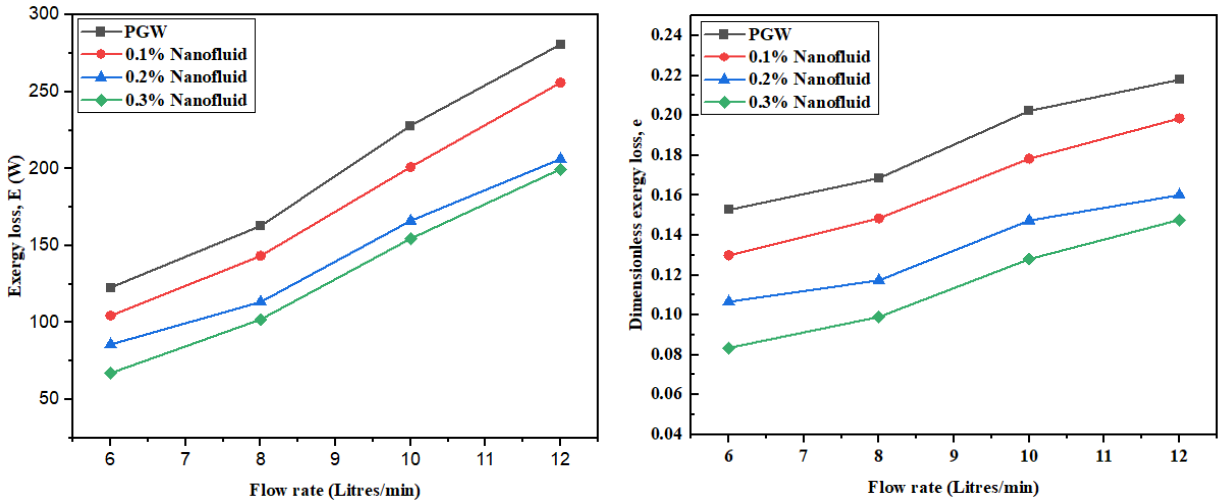

(a) (b)

Figure 14. Changes of (a) exergy loss and (b) dimensional exergy loss with nanofluid flowrate for different nanoparticle volume concentrations.

In Figure 15, the effect of nanoparticle volume concentration and flow rate on exergetic effectiveness is shown. Exergetic effectiveness improved when nanoparticle volume concentration increased and cold fluid flow rate decreased, owing to the reduction in exergy loss. The maximum exergetic effectiveness was observed 29.23% at 0.3% volume concentration of nanofluid when the cold fluid flow rate was 6 liters/min. The average increment of exergatic effectiveness at 0.1%, 0.2%, and 0.3% nanoparticle volume concentration were observed 10.68%, 23.64%, and 31.23% respectively.

Variation of the exergetic sustainability index (SI) by the effect of nanoparticle volume concentration and nanofluid flow rate is shown in Figure 16(a). It was observed that exergetic sustainability index increases with the increment of nanoparticle volume concentration but decreases with the nanofluid flow rate since the exergetic sustainability index is directly proportional to the exergetic effectiveness. The maximum exergetic sustainability index (SI) is 0.41 when nanoparticle concentration is 0.3% and nanofluid flow rate is 6 Litres/min. The environmental impact factor has an inverse relationship with the sustainability index. Figure 16(b) depicts the impact of nanoparticle volume concentration and nanofluid flow rate on the environmental impact factor (EIF). The environmental impact factor decreased as the concentration of nanoparticles increased, but increased with the increment of nanofluid flow rate. The lowest environmental impact factor (EIF) is 2.42 when nanoparticle concentration is 0.3% and nanofluid flow rate is 6 Litres/min. It should be noted that the process/system is more environmentally friendly when the EIF becomes lower value.

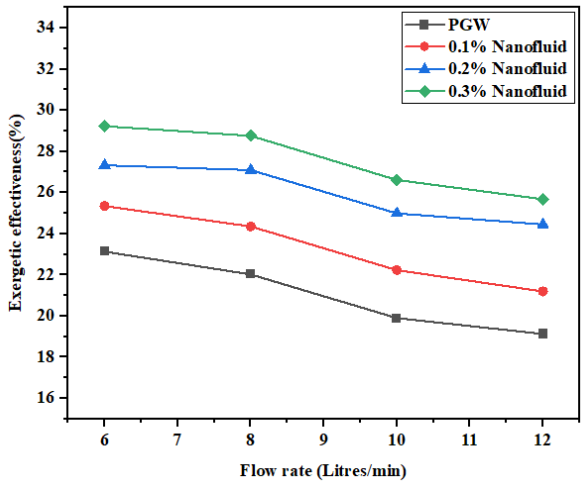

Figure 15. Exergetic effectiveness vs nanofluid flow rate.

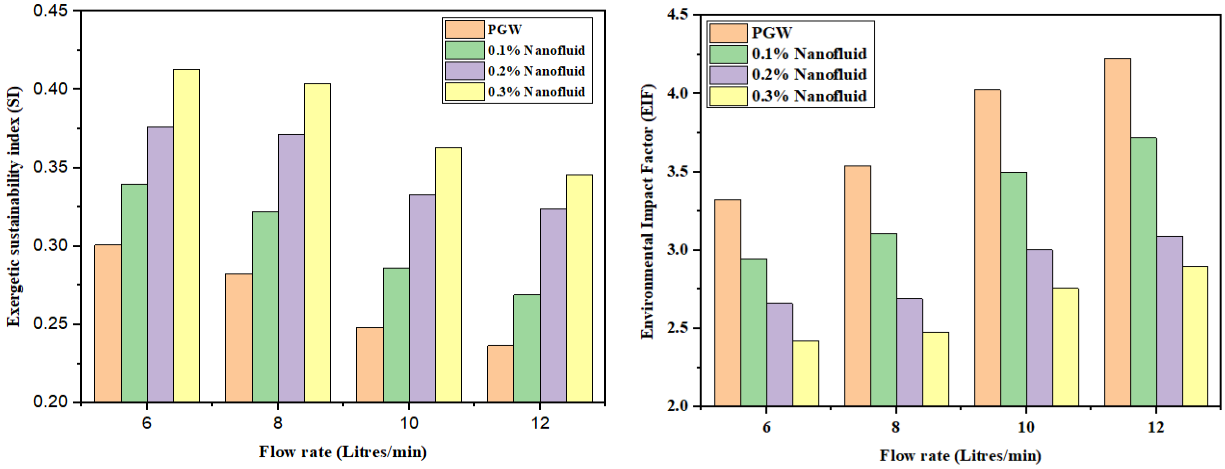

Figure 16. Variation of the (a) sustainability index and (b) environmental impact factor.

CONCLUSION

In this study, ZnO nanoparticles were successfully fabricated and the structural and morphological properties were characterized through X-ray diffraction (XRD) and a scanning electron microscope (SEM). Using PGW-based ZnO Nanofluids instead of PGW as cold fluid on the shell side of the shell and tube heat exchanger resulted in a substantial improvement in energetic and exergetic performance. The following are the key findings:

i. The heat transfer rate and overall heat transfer coefficient increased with the increment of the nanoparticle volume concentration and nanofluid flow rate. Experimental results showed that the maximum heat transfer rate of PGW-based ZnO nanofluid was 464.42 W at 0.3% nanoparticle volume concentration and 12 Liters/min flow rate of nanofluid. When the nanoparticle volume concentration and nanofluid flow rate were 0.3% and 12 Litres/min, respectively, the overall heat transfer coefficient reached its highest value of 1077.06 W/m^{2}K.
ii. The heat exchanger effectiveness was increased with the increment of nanoparticle volume concentration at a certain amount of nanofluid flow.
iii. Exergetic performance in the shell and tube heat exchanger improved as the nanoparticle volume concentration increased, but decreased as the nanofluid flow rate increased.
iv. When the nanoparticle concentration was 0.3% and the nanofluid flow rate was 6 Litres/min, it observed the maximum exergetic sustainability index (0.41) and lowest environmental impact factor (2.42).

According to the results of this experimental analysis, while the amount of heat transfer increased with both the nanoparticle volume concentration and the nanofluid flow rate, the nanofluid (shell side) flow rate should be kept as low as possible to minimize exergy loss and make the process more sustainable and environmentally friendly.

ACKNOWLEDGEMENT

This experimental investigation was conducted in the heat transfer lab of the Department of Mechanical Engineering, CUET. The authors are thankful to Prof. Dr. Md. Mohi Uddin (Department of Physics, CUET) for his co-operations. The authors also gratefully thank to the Solar Energy Technology Research Laboratory of IFRD in BCSIR, Dhaka and Electron Microscopy Laboratory in the Department of Glass and Ceramic Engineering (GCE), BUET.

REFERENCES

[1] K. Narrein and H. A. Mohammed, "Heat transfer and fluid flow characteristics in helically coiled tube heat exchanger (HCTHE) using nanofluids: A review," *J. Comput. Theor. Nanosci.,* vol. 11, no. 4, pp. 911–927, Apr. 2014, doi: 10.1166/jctn.2014.3445.
[2] M. Majid Etghani and S. Amir Hosseini Baboli, "Numerical investigation and optimization of heat transfer and exergy loss in shell and helical tube heat exchanger," *Appl. Therm. Eng.*, vol. 121, pp. 294–301, 2017, doi: 10.1016/j.applthermaleng.2017.04.074.
[3] I. M. Shahrul *et al.*, "Effectiveness study of a shell and tube heat exchanger operated with nanofluids at different mass flow rates," *Numer. Heat Transf.; A: Appl.*, vol. 65, no. 7, pp. 699–713, 2014, doi: 10.1080/10407782.2013.846196.
[4] R. Aghayari *et al.*, "Heat transfer of nanofluid in a double pipe heat exchanger," *Int. Sch. Res. Notices*, vol. 2014, pp. 1–7, Nov. 2014, doi: 10.1155/2014/736424.
[5] S. U. S. Choi and J. A. Eastman, "Enhancing thermal conductivity of fluids with nanoparticles," in *Developments and applications of non-newtonian flows*, D.A. Siginer and H.P. Wang, Eds., New York: ASME, vol. 66, pp. 99-105, 1995.
[6] S. Devireddy, C. S. R. Mekala, and V. R. Veeredhi, "Improving the cooling performance of automobile radiator with ethylene glycol water based TiO_2 nanofluids," *Int. Commun. Heat Mass Transf.* vol. 78, pp. 121–126, Nov. 2016, doi: 10.1016/j.icheatmasstransfer.2016.09.002.
[7] G. Sekrani and S. Poncet, "Ethylene- and propylene-glycol based nanofluids: A litterature review on their thermophysical properties and thermal performances," *Appl. Sci.*, vol. 8, no. 11, pp. 2311, 2018, doi: doi.org/10.3390/app8112311.

[8] Y. Jiang and X. Zhou, "Analysis of flow and heat transfer characteristics of nanofluids surface tension driven convection in a rectangular cavity," *Int. J. Mech. Sci.*, vol. 153–154, pp. 154-163, April 2019, doi: 10.1016/j.ijmecsci.2019.01.034

[9] A. K. Tiwari, P. Ghosh, and J. Sarkar, "Particle concentration levels of various nanofluids in plate heat exchanger for best performance," *Int. J. Heat Mass Transf.* vol. 89, pp. 1110–1118, May 2015, doi: 10.1016/j.ijheatmasstransfer.2015.05.118.

[10] M. M. Sarafraz, F. Hormozi, and V. Nikkhah, "Thermal performance of a counter-current double pipe heat exchanger working with COOH-CNT/water nanofluids," *Exp. Therm. Fluid Sci.* vol. 78, pp. 41–49, 2016, doi: 10.1016/j.expthermflusci.2016.05.014.

[11] R. Martínez-Cuenca *et al.*, "Forced-convective heat transfer coefficient and pressure drop of water-based nanofluids in a horizontal pipe," *Appl. Therm. Eng.*, vol. 98, 2016, pp. 841-849, doi: 10.1016/j.applthermaleng.2015.11.050.

[12] S. E. Abd Elhafez, E. M. Abo-Zahhad, A. H. El-Shazly, and M. F. El-Kady, "Experimental Investigate of Heat transfer for Graphene/Water Nanofluid in Micro heat Exchanger," *AIP Conference Proceedings*, 1814, 020014, 2017. doi: 10.1063/1.4976233.

[13] M. Ghanbarpour, R. Khodabandesh, and K. Vafai, "An investigation of thermal performance improvement of a cylindrical heat pipe using Al_2O_3 nanofluid," *Heat Mass Transfer*, vol. 53, pp. 973–983, 2017, doi: 10.1007/s00231-016-1871-9.

[14] K. Palanisamy and P. C. Mukesh Kumar, "Experimental investigation on convective heat transfer and pressure drop of cone helically coiled tube heat exchanger using carbon nanotubes/water nanofluids," *Heliyon*, vol. 5, no. 5, May 2019, doi: 10.1016/j.heliyon.2019.e01705.

[15] M.M. Elias *et al.*, "Effect of nanoparticle shape on the heat transfer and thermodynamic performance of a shell and tube heat exchanger," *Int. Commun. Heat Mass Transf.*, vol. 44, 2013, pp. 93-99, doi: 10.1016/j.icheatmasstransfer.2013.03.014.

[16] B. Farajollahi, S. Gh. Etemad, and M. Hojjat, "Heat transfer of nanofluids in a shell and tube heat exchanger," *Int. J. Heat Mass Transf.*, vol. 53, pp. 12–17, 2010, doi: 10.1016/j.iheatmasstransfer.2009.10.019.

[17] M. Fares, M. AL-Mayyahi, and M. AL-Saad, "Heat transfer analysis of a shell and tube heat exchanger operated with graphene nanofluids," *Case Stud. Therm. Eng.*, vol. 18, 2020, doi: 10.1016/j.csite.2020.100584.

[18] R. Lotfi, A. M. Rashidi, and A. Amrollahi, "Experimental study on the heat transfer enhancement of MWNT-water nanofluid in a shell and tube heat exchanger," *Int. Commun. Heat Mass Transf.*, vol. 39, no. 1, pp. 108–111, Jan. 2012, doi: 10.1016/j.icheatmasstransfer.2011.10.002.

[19] J. Albadr, S. Tayal, and M. Alasadi, "Heat transfer through heat exchanger using Al2O3 nanofluid at different concentrations," *Case Stud. Therm. Eng.*, vol. 1, no. 1, pp. 38–44, Oct. 2013, doi: 10.1016/j.csite.2013.08.004.

[20] A. Ghozatloo, A. Rashidi, and M. Shariaty-Niassar, "Convective heat transfer enhancement of graphene nanofluids in shell and tube heat exchanger," *Exp. Therm. Fluid Sci.*, vol. 53, pp. 136–141, Feb. 2014, doi: 10.1016/j.expthermflusci.2013.11.018.

[21] S. Hossain *et al.*, "Energy, exergy and sustainability analyses of Bangladesh's power generation sector," *Energy Reports*, vol. 6, pp. 868-878, 2020, doi: 10.1016/j.egyr.2020.04.010.

[22] M.E. Abdur Razzaq, J. U. Ahamed, and M.A.M. Hossain, "Effect of TiO_2/MO nano-lubricant on energy and exergy savings of an air conditioner using blends of R22/R600a," *Int. J. Automot. Mech.,* vol. 17, no. 4, pp. 8283–8297, 2020, doi: 10.15282/ijame.17.4.2020.06.0626.

[23] P. Rakesh and D. Ramana, "Energy & exergy analysis of heat exchanger," *Int. J. Sci. Eng. Res*, vol. 4, no. 6, 2013, [Online]. Available: http://www.ijser.org

[24] M. Gojak and T. Bajc, "Thermodynamic sustainability assessment for heating of residential building," *E3S Web of Conferences,* vol. 111, 04028, 2019. doi: 10.1051/e3sconf/201911104028.

[25] A. Durmuş, "Heat transfer and exergy loss in cut out conical turbulators," *Energy Convers. Manag.*, vol. 45, no. 5, pp. 785–796, Mar. 2004, doi: 10.1016/S0196-8904(03)00186-9.

[26] H. Sadighi Dizaji *et al.,* "A comprehensive second law analysis for tube-in-tube helically coiled heat exchangers," *Exp. Therm. Fluid Sci.*, vol. 76, pp. 118-125, Feb. 2016, doi: 10.1016/j.expthermflusci.2016.03.012.

[27] M. A. Khairul *et al.*, "Heat transfer performance and exergy analyses of a corrugated plate heat exchanger using metal oxide nanofluids," *Int. Commun. Heat Mass Transf.*, vol. 50, pp. 8–14, 2014, doi: 10.1016/j.icheatmasstransfer.2013.11.006.

[28] M. R. Esfahani and E. M. Languri, "Exergy analysis of a shell-and-tube heat exchanger using graphene oxide nanofluids," *Exp. Therm. Fluid Sci.*, vol. 83, pp. 100–106, 2017, doi: 10.1016/j.expthermflusci.2016.12.004.

[29] Z. M. Khoshhesab, M. Sarfaraz, and M. A. Asadabad, "Preparation of ZnO nanostructures by chemical precipitation method," *Synthesis and Reactivity in Inorganic, Metal-Organic and Nano-Metal Chemistry*, vol. 41, no. 7, pp. 814–819, Aug. 2011, doi: 10.1080/15533174.2011.591308.

[30] Y. Xuan, Q. Li, and P. Tie, "The effect of surfactants on heat transfer feature of nanofluids," *Exp. Therm. Fluid Sci.*, vol. 46, pp. 259-262, April 2013, doi: 10.1016/j.expthermflusci.2012.12.004.

[31] P. Bindu and S. Thomas, "Estimation of lattice strain in ZnO nanoparticles: X-ray peak profile analysis," *J. Theor. Appl. Phys.*, vol. 8, no. 4, pp. 123–134, Dec. 2014, doi: 10.1007/s40094-014-0141-9.

[32] R.R. Hong, T.Pan, J.Qian, and H. Li, Synthesis and surface modification of ZnO nanoparticles," *Chem. Eng. J.*, vol. 119, pp. 71–81, 2006, doi: 10.1016/j.cej.2006.03.003.

[33] R. V. Vijayalakshmi *et al.*, "Investigations on structural and optical properties of chalcone dendrimer in $Ag@TiO_2$ core–shell nanoparticles," *Appl. Phys. A: Materials Science and Processing*, vol. 124, no. 11, Nov. 2018, doi: 10.1007/s00339-018-2177-1.

[34] V. Mote, Y. Purushotham, and B. Dole, "Williamson-Hall analysis in estimation of lattice strain in nanometer-sized ZnO particles," *J. Theor. Appl. Phys.*, vol. 6, no. 1, Dec. 2012, doi: 10.1186/2251-7235-6-6.

[35] Y. Zhang, M. K. Ram, E. K. Stefanakos, and D. Y. Goswami, "Synthesis, characterization, and applications of ZnO nanowires," *J. Nanomater.*, vol. 2012, no. 20, pp. 01-22, January 2012, doi: 10.1155/2012/624520.

[36] B. C. Pak and Y. I. Cho, "Hydrodynamic and heat transfer study of dispersed fluids with submicron metallic oxide particles," *Exp. Heat Transf.*, vol. 11, no. 2, pp. 151–170, 1998, doi: 10.1080/08916159808946559.

[37] L-P Zhou *et al.*, "On the specific heat capacity of CuO nanofluid." *Adv. Mech. Eng.*, vol. 2010, pp. 1-4, January 2010. doi: 10.1155/2010/172085.

[38] H. W. Chiam, W. H. Azmi, N. M. Adam, and M.K.A.M. Ariffin, "Numerical study of nanofluid heat transfer for different tube geometries – A comprehensive review on performance," *Int. Commun. Heat Mass Transf.*, vol. 86, pp. 60–70, 2017, doi: 10.1016/j.icheatmasstransfer.2017.05.019.

[39] A. H. Abdelrazek *et al.*, "Heat transfer and pressure drop investigation through pipe with different shapes using different types of nanofluids," *J. Therm. Anal. Calorim.*, vol. 139, pp. 1637–1653, 2020, doi: 10.1007/s10973-019-08562-5.
[40] A. R. I. Ali and B. Salam, "A review on nanofluid: preparation, stability, thermophysical properties, heat transfer characteristics and application", *SN Applied Sciences*, vol. 2, no. 10, pp. 1636, doi: 10.1007/s42452-020-03427-1.
[41] A. M. Hussein, R. A. Bakar, K. Kadirgama, and K.V. Sharma, "Experimental measurement of nanofluids thermal properties," *Int. J. Automot. Mech.*, vol. 7, no. 1, pp. 850–863, 2013, doi: 10.15282/ijame.7.2012.5.0070.
[42] L. S. Sundar *et al.*, "Preparation, thermal and rheological properties of propylene glycol and water mixture based Fe_3O_4 nanofluids," *J. Nanofluids*, vol. 3, no. 3, pp. 200–209, Jul. 2014, doi: 10.1166/jon.2014.1108.
[43] "Propylene glycol based heat-transfer fluids." [Online]. Available: https://www.engineeringtoolbox.com/propylene-glycol-d_363.html [Accessed: May 14, 2021).
[44] J. P. Holman, *Heat Transfer*, 10th ed. New York: The McGraw-Hill Companies, Inc., 2010.
[45] E. Arslan and M. Aktas, "4E analysis of infra red convective dryer powder solar photovoltaic thermal collector," *Sol. Energy*, vol. 208, pp. 46-57, 2020, doi: 10.1016/j.solener.2020.07.071.
[46] U. Seetawan *et al.*, "Effect of calcinations temperature on crystallography and nanoparticles in ZnO disk," *Mater. Sci. Appl.*, vol. 2, no. 9, pp. 1302-1306, 2011, doi: 10.4236/msa.2011.29176.
[47] A. A. Mohamad *et al.*, "First-principles calculation on electronic properties of zinc oxide by zinc–air system," *J. King Saud Univ. Eng. Sci.*, vol. 29, no. 3, pp. 278–283, Jul. 2017, doi: 10.1016/j.jksues.2015.08.002.
[48] H. T. Jarrah, S. S. Mohtasebi, E. Ettefaghi, and F. Jaliliantabar, "Experimental investigation of silver/ water nanofluid heat transfer in car radiator," *J. Mech. Eng. Sci.*, vol. 15, no. 1, pp. 7743-7753, 2021, doi: 10.15282/jmes.15.1.2021.10.0610.